Geomechanics and Engineering, *Vol. 39, No. 1 (2024) 43-54*
https://doi.org/10.12989/gae.2024.39.1.043

Influence of cross-flaws on crack initiation and failure modes around a horseshoe-shaped cavity

Bo Zhang[1,2], Jiancheng Zhang*[1,2], Piaoyang Zhu[3], Jinglong Li**[1], Biao Li[1,2] and Haibo Li[4]

[1]*School of Civil Engineering, Shandong University, Jinan, Shandong 250061, P.R. China*
[2]*School of future technology, Shandong University, Jinan, Shandong 250002, P.R. China*
[3]*Sinic Holdings (Group) - Shanghai and Jiangsu, Suzhou, Jiangsu 215000, P.R. China*
[4]*The Fourth Prospecting of Shandong Coal Geology Bureau, Weifang, Shandong 261000, P.R. China*

(*Received December 12, 2023, Revised August 10, 2024, Accepted September 21, 2024*)

Abstract. Cross-flaws are frequently encountered in practical rock engineering projects near horseshoe-shaped cavities, and their presence can significantly impact the failure mode of these cavities. This study utilizes a combination of laboratory experiments and numerical simulations to investigate the influence of cross-flaws on the failure mode of a horseshoe-shaped cavity. During the experimental tests, we varied the length of secondary flaw and the angle of the cross-flaws in the specimens, followed by subjecting them to biaxial compression. Our experimental results show that when the angle α between the primary and the secondary flaws is small (0° and 45°), only one crack is initiated at the vault of the cavity, resulting in a shear failure mode. Conversely, when the angle α is large (90° and 135°), two cracks are more likely to initiate at the vault of the cavity, leading to the failure mode of falling blocks in the surrounding rock. Furthermore, the circumferential stress at the cavity vault from numerical simulations results is consistent with this observed phenomenon. When the angle α is small, only one circumferential tensile stress concentration is observed at the cavity vault, resulting in the initiation of a single crack. In contrast, when the angle α is large, two stress concentrations appear at the vault of the cavity, leading to the initiation of two cracks from these locations.

Keywords: circumferential tensile stress; crack initiation; cross-flaws; horseshoe-shaped cavity; failure mode

1. Introduction

With the continuous development of large-scale projects, such as deep mining, highway and railway construction, and inter-basin water transfer in China, the demand for tunnel construction is on the rise (Li *et al*. 2016, Feng *et al*. 2022, Ding *et al*. 2019). Disturbances induced during tunnel construction can lead to phenomena such as crack propagation, rock disintegration, fracture, and bending of the arch, posing a risk of rockfall or even collapse within the tunnel (Sagong *et al*. 2011, Li *et al*. 2022, Ying *et al*. 2022, Tao *et al*. 2022a, Ding *et al*. 2023, Shi *et al*. 2023). Consequently, it is crucial to investigate the rock stability and failure modes during excavation and use preventive measures to avoid such disasters. Excavating an underground tunnel leads to changes in the stability of the surrounding rocks (Kun *et al*. 2013, Soomro *et al*. 2023, Jia *et al*. 2017, Tao *et al*. 2022b). Factors such as rock properties, stress-strain states, and vibration disturbances can also affect the tunnel stability (Kumar *et al*. 2022, Xu *et al*. 2020, Lee *et al*. 2018, Tao *et al*. 2019, Zhang *et al*. 2023a, Tao *et al*. 2021). During the excavation and operations of the tunnel, it is of significance to understand its stability and potential failure modes.

Joints and adjacent flaws are factors that influence the properties of the surrounding rock. Crack generated during the damage and failure process is defined as “crack”. When external stresses change, the pre-existing flaws in the rocks can develop into macroscopical split flaws (Li *et al*. 2014). Numerous researchers have investigated the failure modes of individual flaws and concluded that factors such as their angle, length, and loading pattern can influence crack propagation (Zhang and Wong 2012). In specimens with multiple flaws, variables like the angle and distance between flaws can influence crack initiation and propagation, potentially altering the failure mode of the flaws (Wang *et al*. 2020, Vásárhelyi and Bobet 2000, Karimi *et al*. 2021, Tao *et al*. 2020).

The failure mechanism and crack propagation in the surrounding rocks of underground tunnels are affected by the shape and orientation of the tunnels, as well as the interaction of multiple tunnels (Huang *et al*. 2018, Lin *et al*. 2020, Shi *et al*. 2024). When there are flaws or joints above the tunnel, the failure mode of the rock above the tunnel can also change. In an extensive series of experiments, Bieniawski *et al*. (1967) demonstrated that the failure process of rocks is gradual, encompassing successive stages of closure, initiation, extension, and coalescence of internal cracks within the rock. Hoek and Brown (1980) proposed a strength criterion based on statistical analysis of experimental and field data involving various rocks under different confining stresses. Paraskevopoulou *et al*. (2017)

*Corresponding author, Ph.D.
E-mail: zhangjc0760@163.com
**Corresponding author, Ph.D.
E-mail: 215549020@qq.com

ISSN: 2005-307X (Print), 2092-6219 (Online)

confirmed that crack development is the primary cause of stress relaxation. Grendas *et al*. (2018) established correlations between engineering geological features, as classified by the geological strength index, and landslide characteristics. Brady and Brown (2006) explored the strength and deformability of both isotropic and anisotropic rocks through uniaxial and multiaxial compression tests, elaborating on isotropic rock strength criteria and discussing the characteristics of deformability in discontinuous rock masses. Walton *et al*. (2018) investigated the influence of artificial joints on granite properties using triaxial compression tests, analyzing parameters related to brittle cracking and post-yield dilatancy, which enabled qualitative assessment of slope instability. Ding *et al*. (2017) examined tunnel stability in weak rocks and observed that surrounding rock joints compromised tunnel stability, necessitating improved reinforcement methods beyond traditional approaches. Deng *et al*. (2018) studied the impact of overlying rock integrity on cave collapse processes.

Numerous studies have examined the impact of joints and flaws on tunnel stability and failure modes. Jia *et al*. (2008) utilized the finite element method to analyze how different azimuth and lateral pressure coefficients of layered joints weaken jointed rock tunnel stability. Zhu *et al*. (2015) investigated the principal stress direction's influence on intact and cracked tunnel stability, revealing that a 135° angle between the flaw and tunnel spandrel corresponds to the worst rock strength and quality evaluation indexes. Haeri *et al*. (2018) conducted experiments to test fracture toughness in rock specimens with flaws, confirming their reliability using the traditional Brazilian disc method. Cao *et al*. (2016) noted that jointed rock specimen failure modes mainly correlate with joint inclination and angle. Cheng *et al*. (2019) observed that increasing the length of a single flaw leads to decreased peak stress under uniaxial loading, shifting the specimen's failure mode from shear to tensile failure. Jiang *et al*. (2019) employed digital imaging to analyze uniaxial strength, crack propagation mode, and crack initiation angle in specimens with a single flaw, noting that the crack propagation angle initially decreases and then increases with the flaw angle's increase. Zhao *et al*. (2019) investigated the relationship between strain field and crack propagation in specimens with a single flaw, finding that flaw angle influences initial stress and peak strength. Pan *et al*. (2019) explored the impact of filling conditions on crack initiation and propagation, highlighting the stiffness of the filling material and flaw angle as main influencing factors. Zhang *et al*. (2023b) studied the effect of flaw length and distance on crack propagation, noting that under uniaxial and biaxial compression conditions, new cracks near horseshoe-shaped tunnels are initiated from the tunnel rather than from adjacent flaws.

Complex flaws in rocks also play an essential role in the stability of rock masses. Huang *et al*. (2017) conducted a series of uniaxial compression tests on granite specimens containing three non-coplanar holes. They found that the first crack consistently initiated from the surfaces of the pre-existing holes, while secondary cracks originated from either the hole surfaces or other locations within the specimen. Xu *et al*. (2017) studied damage evolution and crack propagation in rocks and concluded that flaw shapes and the interaction between flaws have a great influence on the failure mechanism. Zhou *et al*. (2017) investigated the failure modes of marble specimens with different cavity configurations under uniaxial compression. The results indicated that both the number and layout of cavities significantly influence the mechanical behavior of marble specimens. Wang *et al*. (2017) analyzed the influence of the number and angle of pre-existing flaws on crack propagation through biaxial loading tests. They found that wing flaws play a critical role in propagation and categorized rock bridge failures as wing flaws, secondary shear cracks between horizontal pre-existing flaws, and secondary shear cracks between vertical pre-existing flaws. Zhou *et al*. (2019) and Cheng *et al*. (2016) studied the failure modes of rock specimens with three flaws under uniaxial compression and discussed the influence of rock bridge angle on the mechanical properties and crack propagation of the specimens. Pan *et al*. 2019 and Huang *et al*. 2016 explored the failure behavior of specimens with non-parallel double flaws and revealed that the strength of the specimens decreased as the crack inclination increased under two different crack inclinations.

Numerous scholars have utilized numerical techniques to explore the stability of rock masses with existing flaws. Huang *et al*. (2016) employed PFC software to simulate the failure mode of a rock-like sample containing two non-parallel flaws and extensively analyzed crack initiation, propagation, and coalescence. Zhou *et al*. (2015) simulated the failure process of rock samples with four defects under uniaxial compression using a meshless numerical approach. Their research revealed that crack coalescence follows the path of least resistance among all available paths between any two flaws. Li *et al*. (2015) formulated a constitutive model suitable for brittle rock based on fracture mechanics theory and validated it through experimental tests. Wang *et al*. (2019) similarly utilized PFC to model the failure mode of samples with two coplanar flaws under uniaxial compression, examining the impact of flaw angle, length, and width, as well as rock bridge length, on the failure characteristics of the samples.

Previous research has investigated the failure modes of underground tunnels with flaws through experiments and numerical simulations, as well as the impacts of natural flaws and weak interfaces. However, the influence of cross-flaws around horseshoe-shaped tunnels on crack initiation and failure modes remains insufficiently examined. However, a large number of cross-flaws exist in natural rocks or rock masses (Fig. 1). In this work, we focus on the influence of the angle α between primary and secondary flaws and the length L of the secondary flaw on the failure modes of horseshoe-shaped tunnels.

The structure of this paper is as follows: Section 2 describes the experimental apparatus and sample preparation. Section 3 presents the experimental results and Section 4 introduces the numerical methods and presents the simulation results. Discussions are presented in Section 5 and conclusions of this study are drawn in Section 6.

Fig. 1 Rock mass containing cross-flaws

2 Experimental apparatus and specimen preparation

In this research, a rock-like material was employed to simulate the properties of actual rock formations (Zhang *et al*. 2015, Komurlu *et al*. 2017). The material resembling rock comprises a mixture of cement, sand, and water, combined in a ratio of 1:7.25:1.3 by mass. Grade #325 Portland cement was used, along with fine sand particles smaller than 1.25 mm. This rock-like material demonstrates an uniaxial compressive strength of 7. and a tensile strength of 0.18 MPa.

The experiment entails applying biaxial compression to specimens featuring horseshoe-shaped cavities and cross-flaws. It aims to investigate how the length of secondary flaws and the angle of cross-flaws influence the failure modes of horseshoe-shaped cavities. Tunnels, constructed within geological formations to facilitate underground passage, typically comprise road and railway tunnels, predominantly featuring a horseshoe-shaped cross-section (Dutta *et al*. 2022, Panji *et al*. 2022). This profile offers distinct advantages over circular tunnel sections, showcasing reduced curvature of side arches and invert, resulting in enhanced load-bearing capacity and increased lateral span. Furthermore, the horseshoe-shaped design provides a more expansive environment compared to circular profiles, facilitating large-scale mechanical construction. Recent studies have highlighted significant disparities in the behavior of horseshoe-shaped tunnels compared to circular tunnels under dynamic and static loading conditions (Lu *et al*. 2015, Rahaman *et al*. 2020, Ng *et al*. 2018). Horseshoe-shaped tunnels more accurately reflect the response of real-world tunnel engineering, thereby holding practical significance for the safe construction of numerous tunnels adopting this profile.

The specimen's dimensions are 150 mm × 150 mm × 150mm, as shown in Fig. 2. The cavity's shape mimics a horseshoe, traversing the specimen. It stands at 29.1 mm tall and 38.2 mm wide, with its apex 60 mm from the specimen's upper edge. The cross-flaws are exposed with a 1mm thickness. The highest point of the cavity is 30 mm away from the cross-flaws' intersection, with the angle between the primary flaw and the horizontal direction fixed at 45°, and the primary flaw's length set at 40 mm. Here, L denotes the length of the secondary flaw, and α signifies the angle between the primary and secondary flaws.

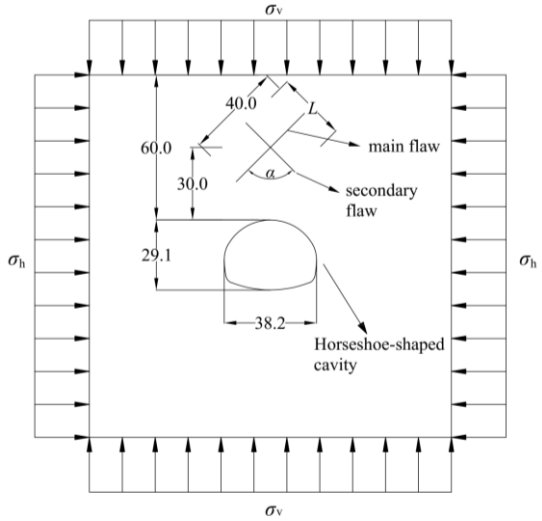

Fig. 2 Schematic of the specimen model, (unit: mm)

The specimen preparation process is as follows:

1) Sand is sieved through a 1.25 mm mesh to remove particles larger than 1.25 mm in diameter.

2) Cement, sand, and water are mixed according to the specified mass ratio and stirred for 10 minutes.

3) The mold model of the horseshoe-shaped cavity is inserted into the specimen mold.

4) The cement, sand, and water mixture is poured into the assembled mold and evenly shaken. It is then left at room temperature for 6 hours to allow the cement mortar to initially set.

5) To create through cracks in the specimen, after the cement mortar initially solidifies, a 0.5 mm thick and 200 mm long blade is inserted into the designated position of the specimen. After 5 minutes, the blade is removed, and the cavity mold is extracted.

6) The specimen is left for final setting for 12 hours. After this period, it is removed from the mold and placed in a curing box, where it is kept for 28 days at a relative humidity of 95% and a temperature of 20 ± 1.5 ℃.

The specimens were categorized into ten testing conditions, as listed in Table 1. The study examined the impacts of secondary flaw length (L), the angle (α) between the primary and secondary flaws, and the confining stress on crack initiation and propagation above the cavity.

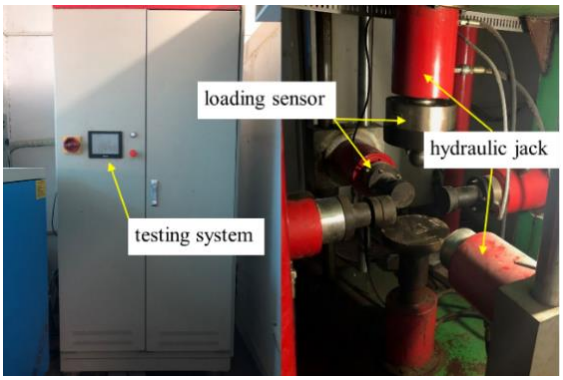

(a) True triaxial test device

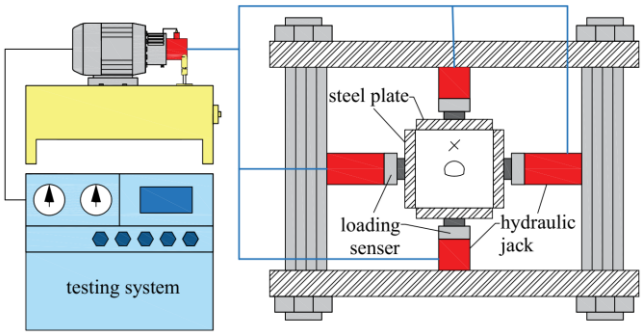

(b) Schematic diagram of triaxial compression

Fig. 3 True triaxial test system

Table 1 Geometric dimensions of flaws and specimens

No.	Loading Mode	α/°	L/mm
1#	biaxial	0	—
2#		45	20
3#			30
4#			40
5#		90	20
6#			30
7#			40
8#		135	20
9#			30
10#			40

Among all specimens, those in testing condition 1 have no secondary flaws, so the angle α between the primary and the secondary flaws in this group is 0°. Additionally, three specimens were subjected to identical parameters and conditions. If at least two specimens exhibited the same failure mode, it was deemed the failure mode for these testing conditions. If the failure modes of all three specimens differed, another set of three specimens with identical parameters was retested until consistent failure modes were determined.

The specimens were subjected to biaxial loading (σ_v and σ_h) using a true triaxial device, as depicted in Fig. 3. Initially, a horizontal stress (σ_h) of 0.67 MPa was applied, followed by the application of vertical stress (σ_v) until failure occurred. Steel plates were inserted between the loading surface of the specimen and the loading frame prior to loading. Vaseline was applied to the contact surfaces of the steel plates and the specimen to minimize friction. To prevent contact between the vertical and horizontal steel plates during loading, the horizontal steel plate measured 150 mm × 150 mm × 20 mm, while the vertical steel plate measured 150 mm × 146 mm × 20 mm. Consequently, the top steel plate was 4 mm shorter than the specimen length, leaving a 2 mm gap between the top steel plate and the two vertical steel plates.

Fig. 4 Crack initiation in specimen 1#

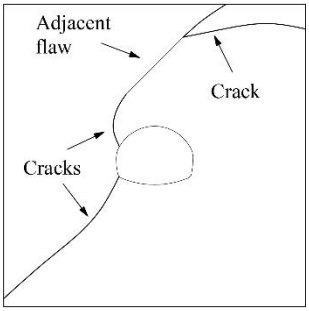

Fig. 5 Schematic of crack propagation in specimen 1#

3. Experimental results and analysis

3.1 Biaxial compression tests of specimens with an adjacent flaw

Biaxial loading tests were performed on specimens without secondary flaws, and crack initiation and propagation in these specimens are shown in Figs. 4 and 5.

It can be observed from the figures that when the angle α between the primary flaw and the secondary flaw is 0°, indicating that the specimens contain only the primary flaw, only one crack is initiated from the vault of the cavity. In the case of biaxial compression, the crack connects with the near tip of the adjacent flaw and then propagates along the upper tip of the adjacent flaw toward the deeper surrounding rock.

(a) α=45°, L=20mm (b) α=45°, L=30mm (c) α=45°, L=40mm

(d) α=90°, L=20mm (e) α=90°, L=30mm (f) α=90°, L=40mm

(g) α=135°, L=20mm (h) α=135°, L=30mm (i) α=135°, L=40mm

Fig. 6 Crack initiation in specimens with cross-flaws under biaxial compression

3.2 Tests of specimens with cross-flaws under biaxial compression

Figs. 6 and 7 present the results from nine specimens subjected to biaxial compression tests with varying parameters. It is evident that, under biaxial compression conditions, when the angle α between the primary flaw and the secondary flaw is 45°, only one crack is initiated at the vault of the cavity. However, when the angle α is 90° and 135°, it is more likely to have two cracks initiated at the vault of the cavity. Specifically, when the angle α is 45°, and the secondary flaw length L is 30 mm and 40 mm, only one crack is initiated at the vault of the cavity.

The crack deflects towards the cross-flaws and intersects with the secondary flaw, as illustrated in Figs. 6 and 7(a)-7(c). In cases where the secondary flaw length (L) is 20 mm, only one crack initiates at the vault of the cavity, being drawn towards the tip of the primary flaw, as depicted in Figs. 6 and 7(a), 7(d), and 7(g). A rupture area is created near the cross-flaws under these testing conditions.

When α is 90° and L is 30 mm and 40 mm, two cracks initiate at the cavity's vault. They propagate towards the cross-flaws, intersecting with nearby tips of the primary and secondary flaws, as shown in Figs. 6 and 7(e), 7(f). For α of 135° and L of 30 mm or 40 mm, two cracks initiate from the cavity's vault and propagate vertically towards the cross-flaws. Eventually, one crack connects with the nearby tip of the primary flaw, while the other connects with the intersection of the cross-flaws, as depicted in Figs. 6 and 7(h), 7(i). Finally, under these two testing conditions, a block-shaped cutting body is created between the cavity and the cross-flaws, which could pose a danger in practical engineering.

The experimental results show that, under biaxial compression, if the secondary flaw length is short (e.g., L is 20mm), regardless of the angle α, the primary flaw is more attracted to the cracks than the secondary flaw, and the cracks make contact with the near tip of the primary flaw.

As the length L increases (e.g., L is 30 mm and 40 mm), and the angle α is 45°, the secondary flaw is more attracted

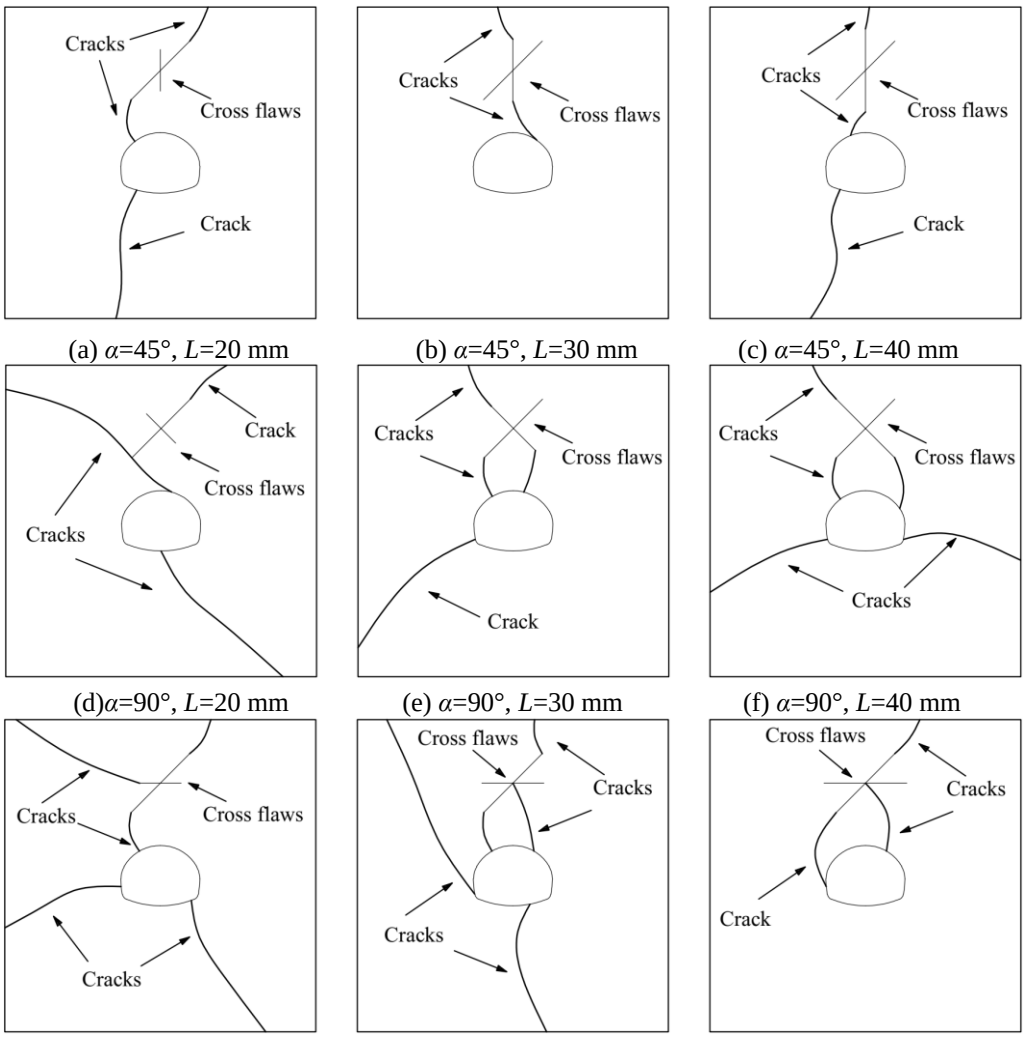

(a) α=45°, L=20 mm (b) α=45°, L=30 mm (c) α=45°, L=40 mm

(d)α=90°, L=20 mm (e) α=90°, L=30 mm (f) α=90°, L=40 mm

(g) α=135°, L=20 mm (h) α=135°, L=30 mm (i) α=135°, L=40 mm

Fig. 7 Crack initiation occurred in specimens containing cross-flaws under biaxial compression. Thin lines depict cavities and adjacent flaws, while thick lines illustrate crack propagation paths. Figures (a) through (i) correspond to specimens 2# through 10#, respectively

to the cracks than the primary flaw, and the cracks are easier to contact the near tip of the secondary flaw. These testing conditions result in a rupture area near the cross-flaws. Furthermore, under the testing conditions of α being 90° and 135°, when the secondary flaw length L is 30 mm and 40 mm, under the influence of the cross-flaws, two parallel cracks are easily formed, and a block-shaped cutting body is generated between the cavity and the cross-flaws. In practical engineering projects, the surrounding rock at the vault of the cavity is prone to significant collapses and block falls, potentially leading to accidents

4. Numerical analyses of crack initiation

It can be observed from the tests mentioned above that under biaxial compression, the number of initiation points above the horseshoe-shaped cavity is related to the form and parameters of the cross-flaws. We employed the numerical software ABAQUS to simulate three specimen models for analyzing these experimental phenomena. The advancement of the finite element method has expanded opportunities for investigating diverse properties of rock-like materials (Zhang *et al*. 2020). However, conventional finite element methods prove ineffective in addressing nonlinear issues like crack propagation in such materials. XFEM, with its introduction of discontinuous displacement modes, enables the handling of discontinuous fields irrespective of mesh boundaries. This methodology mitigates mesh restructuring challenges and substantially diminishes the numerical simulation's reliance on mesh quality, presenting significant advantages in simulating crack propagation (Zhang *et al*. 2023a). Hence, this study employs XFEM to model the initiation and propagation of cracks in specimens subjected to biaxial compression conditions. The rock-like material has an elastic modulus of 233 MPa, a Poisson's ratio of 0.18, a horizontal stress (σ_h) of 0.67 MPa, and a vertical stress (σ_v) of 6.7 MPa.

We used Abaqus to calculate the stress distribution above the cavity of the specimen. The simulation results are shown in Fig. 8.

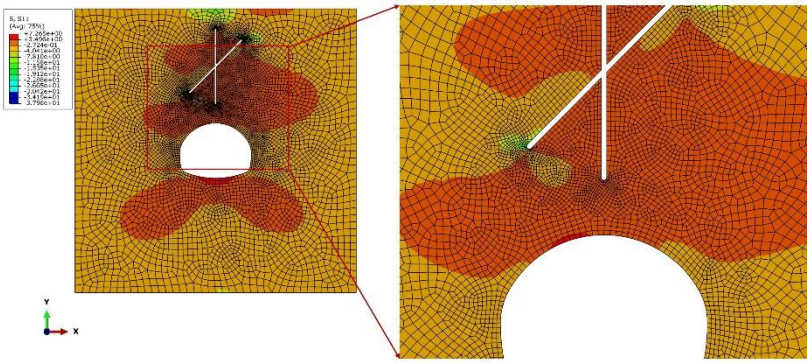

(a) stress contour in the x direction

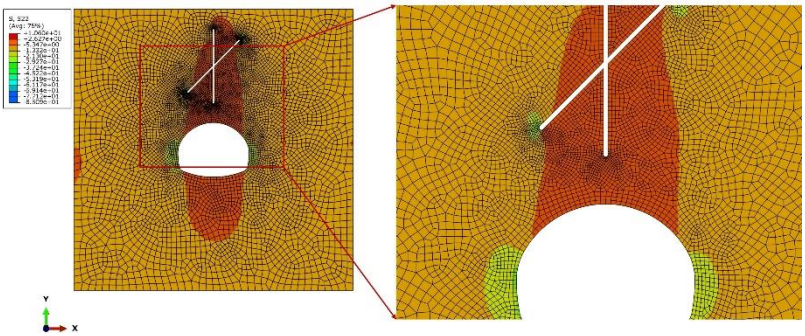

(b) stress contour in the y direction

Fig. 8 Numerical simulation results of stress contour for test specimens 4#

Fig. 8 illustrates the stress contour results for specimen 4#. Horizontal and vertical stress concentrations exist between the top of the cavity and the cross-flaws. The stress at this position cannot be accurately characterized by horizontal and vertical stresses due to the cavity's vault being a circular arc with a radius of 20.2 mm. Thus, we calculated the circumferential stress at the cavity's vault by establishing a local polar coordinate system. The results of circumferential stress are shown in Fig. 9. Then, we extracted the circumferential stress data of the partial nodes of the vault and plotted the circumferential stress curve of the cavit vault. The results are shown in Fig. 10.

From Figs. 9 and 10, we can see a maximum value of circumferential tensile stress at the vault of the cavity in testing conditions 1# and 4#. In contrast, there are two stress concentrations under testing conditions 7# and 9#. The cavity is most likely to fail at the location with the highest circumferential tensile stress concentration. Therefore, if there is only one maximum circumferential tensile stress concentration, tensile damage occurs at the corresponding position of the specimen, leading to the initiation of a single crack at the cavity's vault. When there are two maximum stress concentration points, tensile damage occurs at these two corresponding positions. Consequently, two cracks are likely to initiate at the cavity's vault.

The cavity is most likely to begin to fail at the point where the circumferential tensile stress concentration is the highest. Therefore, when there is only one maximum circumferential tensile stress concentration, tensile damage occurs at the corresponding position of the specimen, and only one crack is likely to initiate at the vault of the cavity.

When there are two maximum stress concentration points, tensile damage occurs at these two corresponding positions. As a result, two cracks are likely to initiate at the vault of the cavity.

From this, we can infer that under biaxial loading, when the angle α is small (0° and 45° in this study), the circumferential stress at the vault of the cavity always has only one maximum concentration point, resulting in the initiation of a single crack. In the case of an angle α of 90° and 135°, and when the secondary flaw is long (30 mm and 40mm in this study), the circumferential stress exhibits two maximum concentrations at the cavity's vault. This leads to the initiation of two cracks propagating toward the direction of the maximum principal stress. These simulation results are consistent with the experimental findings.

5. Discussion

Scholarly research has extensively investigated crack initiation, propagation, and failure modes in specimens with adjacent flaws. For example, Huang *et al.* (2017) conducted uniaxial compression tests on granite specimens with three non-coplanar holes. They observed that initial cracks consistently originated from hole surfaces, while secondary cracks initiated from either hole surfaces or specific locations on the specimen's intact part. Wang *et al.* (2017) investigated the influence of the number and angle of pre-existing flaws on crack propagation in biaxial loading tests. They discovered that wing flaws play a critical role in the propagation process. Zhang *et al.* (2023b) studied the impact of adjacent flaws on crack initiation and

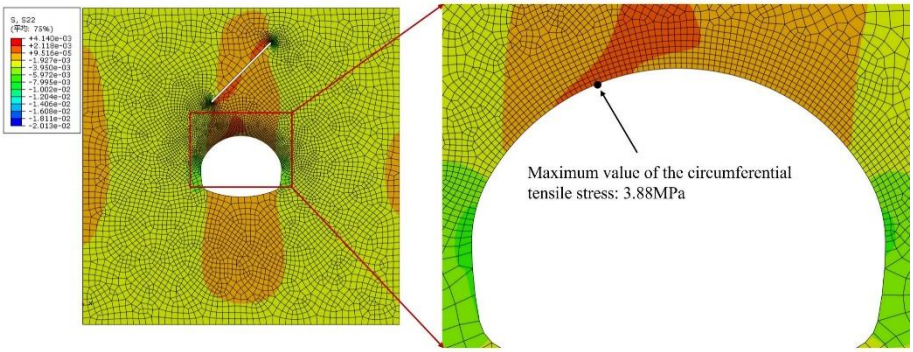

(a) α=0°

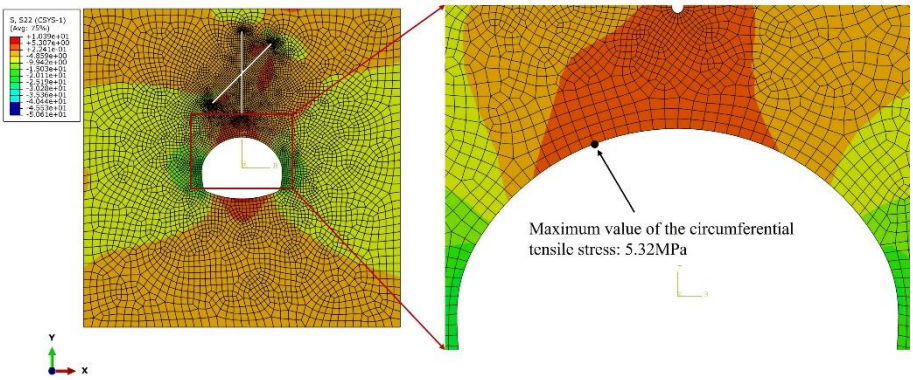

(b) α=45°, L=40mm

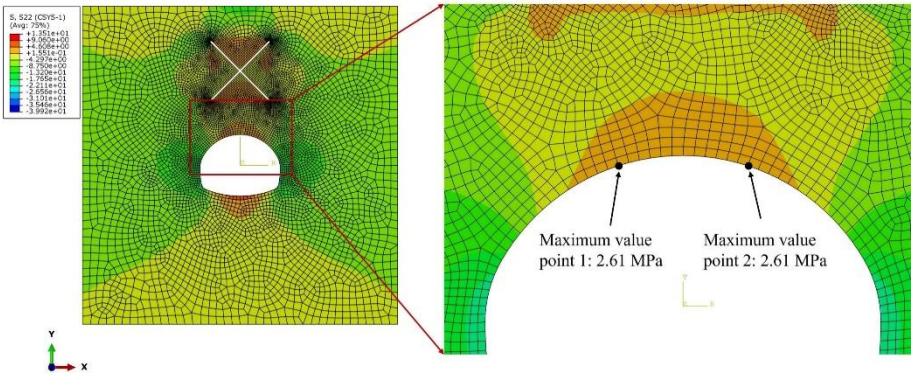

(c) α=90°, L=40 mm

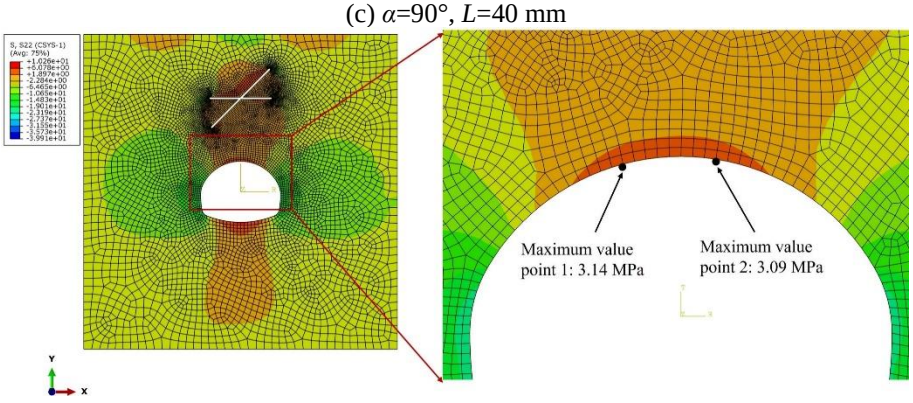

(d) α=135°, L=30 mm

Fig. 9 Simulation results of the circumferential stress at the vault of the horseshoe-shaped cavity under biaxial compressio n. Figures (a), (b), (c), and (d) are for specimens 1#, 4#, 7# and 9#, respectively

propagation. They noted that new cracks originated from the cavity rather than the adjacent flaw. Zhou *et al*. (2019) examined the failure mode of rock masses with three flaws under uniaxial compression. They discussed how the rock bridge angle affects the mechanical properties and crack propagation. Xu *et al*. (2017) analyzed the evolution of rock

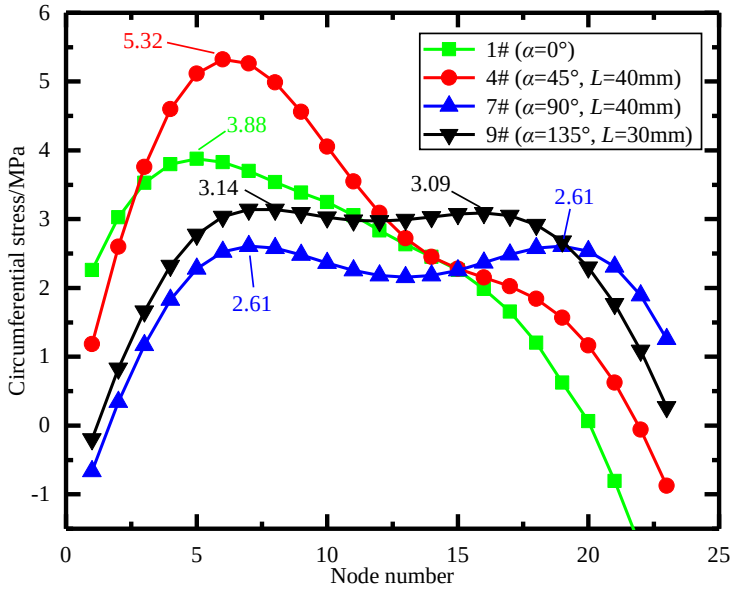

Fig. 10 Circumferential stress curve of the cavity vault under biaxial compression

damage and crack propagation, concluding that flaw shapes and the interaction between flaws significantly influence the failure mechanism.

Currently, investigations have focused on multiple flaws of the same type or flaws with various regular shapes. However, the impact of cross-flaws around horseshoe-shaped cavities on crack initiation and failure modes remains inadequately explored. According to the test results and numerical analyses, crack initiation at the vault of the cavity is associated with the circumferential stress at the vault. The simulation shows that when the angle α between the primary and secondary flaws is small (0° and 45°), there is only one circumferential stress concentration at the cavity vault, consequently, only one tensile stress induced crack is initiated at the vault. The closer the secondary flaw is to the cavity, the easier it is for the crack to propagate towards the secondary flaw in the direction of the principal stress.

However, when the angle α is large (90° and 135°) and the secondary flaw length L is 30 mm or 40 mm, circumferential stress exhibits two concentration points at the cavity vault. This leads to the development of tensile stress induced cracks at two corresponding locations at the vault of the cavity. These two cracks then propagate along the direction of the maximum principal stress, influenced by the presence of cross-flaw tips, ultimately connecting with them. Subsequently, two parallel cracks are generated between the cavity vault and the cross-flaws. This results in the development of a block-shaped cutting body between the cavity vault and the cross-flaws, increasing the risk of sudden falls of the block from the surrounding rock. In summary, conclusion, within practical engineering scenarios, larger values of α and L (i.e., α of 90°, 135° and L of 30 mm, 40 mm) significantly increase the probability of sudden rockfall following the formation of two parallel cracks, leading to potential accidents. Conversely, when the angle α is small, the probability of sudden rock collapse is lower due to the formation of only one crack.

6. Conclusions

In this study, we conducted a thorough investigation into the influence of cross-flaws surrounding horseshoe-shaped cavities on crack initiation and propagation using a combination of experiments and numerical simulations. Additionally, we extensively discussed the failure modes of rock masses under biaxial compression. The main conclusions are summarized as follows.

(1) The angle α between the primary and the secondary flaw influences the circumferential tensile stress around the horseshoe-shaped cavity. When the angle α is large (90° and 135° in this work) and the secondary flaw length L is 30 mm and 40 mm, two circumferential tensile stress concentrations exist above the cavity vault. Conversely, when the angle α is small (0° and 45°), there is only one maximum stress concentration above the cavity vault.

(2) The angle α between the primary and the secondary flaw, as well as the circumferential tensile stress around the horseshoe-shaped cavity, both influence the failure modes around the cavity. When the angle α is large (90° and 135°) and L is 30 mm and 40 mm, two cracks are created from the vault of the cavity, easily cutting the rock mass, resulting in the collapse of a large block-shaped cutting body. When the angle α is small (0° and 45°), only one crack is formed, which does not lead to the formation of a block at the cavity vault.

Acknowledgments

This paper is funded by the National Natural Science Foundation of China (NO. 42272311, 51909142), the Youth program of National Natural Science Foundation of China (No. 52309134), the Youth Foundation of Shandong Province (No. ZR2023QE266).

References

Bieniawski, Z.T. (1967), "Mechanism of brittle fracture of rock, Parts I, II and III", *Int. J. Rock Mech. Min.Sci.*, **4**, 395-430. https://doi.org/10.1016/0148-9062(67)90032-0.

Brady, B.H.G. and Brown, E.T. (2006), "Rock mechanics for underground mining", Springer, *Dordrecht*, https://doi.org/10.1007/978-1-4020-2116-9.

Cao, R.H., Cao, P., Lin, H., Pu, C.Z. and Ou, K. (2016), "Mechanical behavior of brittle rock-like specimens with pre-existing fissures under uniaxial loading: experimental studies and particle mechanics approach", *Rock Mech. Rock Eng.*, **49**(3), 763-783. https://doi.org/10.1007/s00603-015-0779-x.

Cheng, H., Zhou, X., Zhu, J. and Qian, Q. (2016),. "The effects of crack openings on crack initiation, propagation and coalescence behavior in rock-like materials under uniaxial compression", *Rock Mech. Rock Eng.*, **49**(9), 3481-3494. https://doi.org/10.1007/s00603-016-0998-9.

Cheng, X.Y. (2019), "Damage and failure characteristics of rock similar materials with pre-existing cracks", *Int. J. Coal Sci. Technol.*, **6**(4), 505-517. https://doi.org/10.1007/s40789-019-0263-4.

Dutta, P., Bhattacharya, P. and Kumar, A. (2022), "Support pressure for undrained stability of horseshoe-shaped twin tunnels with semi-elliptical roof in clay", *Iran. J. Sci. Technol.-Trans. Civ. Eng.*, **46**(3), 2697-2711. https://doi.org/10.1007/s40996-021-00763-z.

Deng, E., Yang, W.C., Lei, M.F., Yin, R.S. and Zhang, P.P. (2018), "Instability mode analysis of surrounding rocks in tunnel blasting construction with thin bedrock roofs", *Geotech. Geol. Eng.*, **36**(4), 2565-2576. https://doi.org/10.1007/s10706-018-0483-1.

Ding, P., Tao, L., Yang, X., Zhao, J. and Shi, C. (2019), "Three-dimensional dynamic response analysis of a single-ring structure in a prefabricated subway station", *Sust. Cities Soc.*, **45**, 271-286. https://doi.org/10.1016/j.scs.2018. 11.010.

Ding, P., Shi, C., Tao, L., Liu, Z. and Zhang, T. (2023), "Research on seismic analysis methods of large and complex underground pipe structures in hard rock sites", *Tunn. Undergr. Sp. Technol.*, **135**, 105035. https://doi.org/10.1016/j.tust.2023.105035.

Ding, S., Gao, Y., Jing, H., Shi, X., Qi, Y. and Guo, J. (2021), "Influence of weak interlayer on the mechanical performance of the bolted rock mass with a single free surface in deep mining", *Minerals* (*Basel*), **11**(5), 496. https://doi.org/10.3390/min11050496.

Feng, X.J., Wang, P., Liu, S.F., Wei, H., Miao, Y.L. and Bu, S.J. (2022), "Mechanism and law analysis on ground settlement caused by shield excavation of small-radius curved tunnel", *Rock Mech. Rock Eng.*, **55**(6), 3473-3488. https://doi.org/10.1007/s00603-022-02819-6.

Grendas, N., Marinos, V., Papathanassiou, G., Ganas, A. and Valkaniotis, S. (2018), "Engineering geological mapping of earthquake-induced landslides in South Lefkada Island, Greece: evaluation of the type and characteristics of the slope failures", *Environ. Earth Sci.*, **77**(12), 1-19. https://doi.org/10.1007/s12665-018-7598-9.

Haeri, H., Sarfarazi, V., Yazdani, M., Shemirani, A.B. and Hedayat, A. (2018), "Experimental and numerical investigation of the center-cracked horseshoe disk method for determining the mode I fracture toughness of rock-like material", *Rock Mech. Rock Eng.*, **51**(1), 173-185. https://doi.org/10.1007/s00603-017-1310-3.

Hoek, E. and Brown, E.T. (1980), "Empirical strength criterion for rock masses", *J. Geotech. Eng. Div. ASCE*, **106**(9), 1013-1035.

Huang, Y.H., Yang, S.Q., Hall, M.R., Tian, W.L. and Yin, P.L. (2018), "Experimental study on uniaxial mechanical properties and crack propagation in sandstone containing a single oval cavity", *Arch. Civ. Mech. Eng.*, **18**(4), 1359-1373. https://doi.org/10.1016/j.acme.2018.04.005.

Huang, Y.H., Yang, S.Q., Ranjith, P.G. and Zhao, J. (2017), "Strength failure behavior and crack evolution mechanism of granite containing pre-existing non-coplanar holes: experimental study and particle flow modeling", *Comput. Geotech.*, **88**, 182-198. https://doi.org/10.1016/j.compgeo.2017.03.015.

Jiang, T., Pan, X., Lei, J., Zhang, J. and Wang, W. (2019), "Rupture and crack propagation in artificial soft rock with preexisting fractures under uniaxial compression", *Geotech. Geol. Eng.*, **37**(3), 1943-1956. https://doi.org/10.1007/s10706-018-0736-z.

Jia, C., Li, Y., Lian, M.Y. and Zhou, X.Y. (2017), "Jointed surrounding rock mass stability analysis on an underground cavern in a hydropower station based on the extended key block theory", *Energies* (*Basel*), **10**(4), 563. https://doi.org/10.3390/en10040563.

Jia, P. and Tang, C.A. (2008), "Numerical study on failure mechanism of tunnel in jointed rock mass", *Tunn. Undergr. Sp. Technol.*, **23**(5), 500-507. https://doi.org/10.1016/j.tust.2007.09.001.

Karimi, J., Asadizadeh, M., Hossaini, M.F., Nowak, S. and Sherizadeh, T. (2021), "Compressive strength of flawed cylindrical specimens subjected to axial loading", *Geomech. Eng.*, **27**(1), 87-99. https://doi.org/10.12989/gae.2021.27.1.087.

Komurlu, E., Kesimal, A. and Demir, A.D. (2017), "Dog bone shaped specimen testing method to evaluate tensile strength of rock materials", *Geomech. Eng.*, **12**(6), 883-898. https://doi.org/10.12989/gae.2017.12.6.883.

Kumar, A. and Tiwari, G. (2022), "Jackknife based generalized resampling reliability approach for rock slopes and tunnels stability analyses with limited data: Theory and applications", *J. Rock Mech. Geotech. Eng.*, **14**(3), 714-730. https://doi.org/10.1016/j.jrmge.2021.11.003.

Kun, M. and Onargan, T. (2013), "Influence of the fault zone in shallow tunneling: A case study of izmir metro tunnel", *Tunn. Undergr. Sp. Technol.*, **33**, 34-45. https://doi.org/10.1016/j.tust.2012.06.016.

Lee, J. and Hong, J. (2018), "Crack initiation and fragmentation processes in pre-cracked rock-like materials", *Geomech. Eng.*, **15**(5), 1047-1059. https://doi.org/10.12989/gae.2018.15.5.1047.

Lin, Q.B., Cao, P., Cao, R.H., Lin, H. and Meng, J.J. (2020), "Mechanical behavior around double circular openings in a jointed rock mass under uniaxial compression", *Arch. Civ. Mech. Eng.*, **20**(1), 1-18. https://doi.org/10.1007/ s43452-020-00027-z.

Li, H.Q. and Wong, L.N.Y. (2014), Numerical study on coalescence of pre-existing flaw pairs in rock-like material", *Rock Mech. Rock Eng.*, **47**(6), 2087-2105. https://doi.org/10.1007/s00603-013-0504-6.

Li, X.H., Zhu, Z.M., Wang, M., Shu, Y., Deng, S., Xiao, D.J., 2022. "Influence of blasting load directions on tunnel stability in fractured rock mass", *J. Rock Mech. Geotech. Eng.*, **14**(2), 346-365. https://doi.org/10.1016/ j.jrmge.2021.06.010.

Li, X. and Konietzky, H. (2015), "Numerical simulation schemes for time-dependent crack growth in hard brittle rock", *Acta Geotech.*, **10**(4), 513-531. https://doi.org/10.1007/s11440-014-0337-9.

Li, Y.Y., Jin, X. G., Lv, Z.T., Dong, J.H. and Guo, J.C. (2016), "Deformation and mechanical characteristics of tunnel lining in tunnel intersection between subway station tunnel and construction tunnel", *Tunn. Undergr. Sp. Technol.*, **56**, 22-33. https://doi.org/10.1016/j.tust.2016.02.016.

Lu, A., Zhang, N., Zhang, X., Lu, D. and Li, W. (2015), "Analytic method of stress analysis for an orthotropic rock mass with an arbitrary-shaped tunnel", *Int. J. Geomech.*, **15**(4), 04014068.

https://doi.org/10.1061/(ASCE)GM.1943-5622.0000408.

Ng, C. W.W., Fong, K.Y. and Liu, H.L. (2018), "The effects of existing horseshoe-shaped tunnel sizes on circular crossing tunnel interactions: Three-dimensional numerical analyses", *Tunn. Undergr. Sp. Technol.*, **77**, 68-79. https://doi.org/10.1016/j.tust.2018.03.025.

Paraskevopoulou, C., Perras, M., Diederichs, M., Amann, M., Low, S., Lam, T. and Jensen, M. (2017), "The three stages of stress relaxation - Observations for the time-dependent behaviour of brittle rocks based on laboratory testing", *Eng. Geol.*, **216**, 56-75. https://doi.org/10.1016/j.enggeo.2016.11.010.

Pan P.Z., Miao S.T., Jiang Q., Wu Z.H. and Shao C.Y. (2019), "The influence of infilling conditions on flaw surface relative displacement induced cracking behavior in hard rock", *Rock Mech. Rock Eng.*, **53**(10), 4449-4470. https://doi.org/10.1007/s00603-019-02033-x.

Pan, W., Wang, X., Liu, Q., Yuan, Y. and Zuo, B. (2019), "Non-parallel double-crack propagation in rock-like materials under uniaxial compression", *Int. J. Coal Sci. Technol.*, **6**(3), 372-387. https://doi.org/10.1007/s40789-019-0255-4.

Panji, M., Mojtabazadeh-Hasanlouei, S. and Fakhravar, A. (2022), "Seismic response of the ground surface including underground horseshoe-shaped cavity", *Transp. Infrastruct. Geotechnol.*, **9**(3), 338-355. https://doi.org/ 10.1007/ s40515-021-00178-3.

Rahaman, O. and Kumar, J. (2020), "Stability analysis of twin horse-shoe shaped tunnels in rock mass", *Tunn. Undergr. Sp. Technol.*, **98**, 103354. https://doi.org/10.1016/j.tust.2020.103354.

Sagong, M., Park, D., Yoo, J. and Lee, J.S. (2011), "Experimental and numerical analyses of an opening in a jointed rock mass under biaxial compression", *Int. J. Rock Mech. Min. Sci.*, **48**(7), 1055-1067. https://doi.org/10.1016/j. ijrmms.2011.09.001.

Shi, C., Tao, L., Ding, P., Wang, Z. and Jia, Z. (2023), "Study on seismic response characteristics and failure mechanism of giant-span flat cavern", *Tunn. Undergr. Sp. Technol.*, **140**, 105328. https://doi.org/10.1016/j.tust.2023. 105328.

Shi, C., Tao, L., Ding, P., Wang, Z., Jia, Z. and Shi, M. (2024), "Analytical solution for deep non-circular tunnels considering slippage effects under far-field seismic SV waves", *Tunn. Undergr. Sp. Technol.*, **144**, 105552. https://doi.org/10.1016/j.tust.2023.105552.

Soomro, M.A., Mangnejo, D.A. and Mangi, N. (2023), "Investigation of crack growth in a brick masonry wall due to twin perpendicular excavations", *Geomech. Eng.*, **34**(3), 251-265. https://doi.org/10.12989/gae.2023.34.3.251.

Tao, L., Ding, P., Shi, C., Wu, X., Wu, S. and Li, S. (2019), "Shaking table test on seismic response characteristics of prefabricated subway station structure", *Tunn. Undergr. Sp. Technol.*, **91**, 102994. https://doi.org/10.1016/j. tust.2019.102994.

Tao, L., Ding, P., Yang, X., Lin, P., Shi, C., Bao, Y., Wei, P. and Zhao, J. (2020), "Comparative study of the seismic performance of prefabricated and cast-in-place subway station structures by shaking table test", *Tunn. Undergr. Space Technol.*, **105**, 103583. https://doi.org/10.1016/j.tust.2020.103583.

Tao, L., Ding, P., Lin, H., Wang, H., Kou, W., Shi, C., Li, S. and Wu, S. (2021), "Three-dimensional seismic performance analysis of large and complex underground pipe trench structure", *Soil Dyn. Earthq. Eng.*, **150**, 106904. https://doi.org/10.1016/j.soildyn.2021.106904.

Tao, L., Shi, C., Ding, P., Li, S., Wu, S. and Bao, Y. (2022a), "A study on bearing characteristic and failure mechanism of thin-walled structure of a prefabricated subway station", *Front. Struct. Civ. Eng.*, **16**(3), 359-377. https://doi.org/10.1007/s11709-022-0816-2.

Tao, L., Shi, C., Ding, P., Yang, X., Bao, Y. and Wang, Z. (2022b), "Shaking table test of the effect of an enclosure structure on the seismic performance of a prefabricated subway station", *Tunn. Undergr. Sp. Technol.*, **125**, 104533. https://doi.org/10.1016/j.tust.2022.104533.

Vásárhelyi, B. and Bobet, A. (2000), "Modeling of crack initiation, propagation and coalescence in uniaxial compression", *Rock Mech. Rock Eng.*, **33**(2), 119-139. https://doi.org/10.1007/s006030050038.

Wang, M., Wan, W. and Zhao, Y.L. (2020), "Experimental study on crack propagation and the coalescence of rock-like materials with two preexisting fissures under biaxial compression", *Bull. Eng. Geol. Environ.*, **79**(6), 3121-3144. https://doi.org/10.1007/s10064-020-01759-1.

Wang, M., Cao, P., Wan, W., Zhao, Y.L., Liu, J. and Liu, J.S. (2017), "Crack growth analysis for rock-like materials with ordered multiple pre-cracks under biaxial compression", *J. Cent. South Univ.*, **24**(4), 866-874. https://doi.org/10.1007/s11771-017-3489-6.

Walton, G., Alejano, L.R., Arzua, J. and Markley, T. (2018), "Crack damage parameters and dilatancy of artificially jointed granite samples under triaxial compression", *Rock Mech. Rock Eng.*, **51**(6), 1637-1656. https://doi.org/10.1007/s00603-018-1433-1.

Xu, Q., Chen, J.T. and Xiao, M. (2020), "Analysis of unsteady seepage field and surrounding rock stability of underground cavern excavation", *Tunn. Undergr. Sp. Technol.*, **97**, 103239. https://doi.org/10.1016/j. tust.2019.103239.

Xu, J. and Li, Z.X. (2019),." Crack propagation and coalescence of step-path failure in rocks", *Rock Mech. Rock Eng.*, **52**(4), 965-979. https://doi.org/10.1007/s00603-018-1661-4.

Ying, P., Li, W.J., Zhu, Z.M., Li, X.H., Gao, W.T. and Shu, Y. (2022), "Influence of impact loading orientations on the mechanical behaviour of rocks around a tunnel", *Int. J. Rock Mech. Min. Sci.*, **152**, 105071. https://doi.org/10.1016/j.ijrmms.2022.105071.

Zhao, C., Niu, J., Zhang, Q., Zhao, C. and Zhou, Y. (2019), "Failure characteristics of rock-like materials with single flaws under uniaxial compression", *Bull. Eng. Geol. Environ.*, **78**(1), 593-603. https://doi.org/10.1007/s10064-018-1379-2.

Zhang, B., Li, Y., Yang, X.Y., Li, S.C., Wei, C. and Songa, J. (2023a), "Influence of size and location of a pre-existing fracture on hydraulic fracture propagation path", *Geomech. Eng.*, **32**(3), 321-333. https://doi.org/10.12989/gae.2023.32.3.321.

Zhang, B., Zhu, P., Zhang, J., Li, S., Qiu, D. and Li, J. (2023b), "Effect of an adjacent flaw on the crack propagation of a horseshoe-shaped cavity", *Rock Mech. Rock Eng*, **56**(3), 1807-1821. https://doi.org/10.1007/s00603-022-03132-y.

Zhang, B., Li, S.C., Yang, X.Y., Zhang, D.F., Wang Q., CAI W., Yang C.X. and Deng Z.Q. (2015), "Mechanical property of rock-like material with intersecting multi-flaws under uniaxial compression", *J. Rock Mech. Eng.*, **34**(9): 55-63. https://doi.org/10.13722/j.cnki.jrme.2014.0876.

Zhang, B., Li, Y., Yang, X.Y., Li, S.C., Liu, B., Xu, Z.H. and Pei, Y. (2020), "Influence of two cross-flaws geometry on the strength and crack coalescence of rock-like material specimens under uniaxial compression", *Int J Geomech.*, **20**(8). https://doi.org/10.1061/(ASCE)GM.1943-5622.0001757.

Zhang, X. and Wong, L.N.Y. (2012), "Cracking processes in rock-like material containing a single flaw under uniaxial compression: A numerical study based on parallel bonded-particle model approach", *Rock Mech. Rock Eng.*, **45**(5), 711-737. https://doi.org/10.1007/s00603-011-0176-z.

Zhou, X.P., Wang, Y.T., Zhang, J.Z. and Liu, F.N. (2019), "Fracturing behavior study of three-flawed specimens by uniaxial compression and 3D digital image correlation: sensitivity to brittleness", *Rock Mech. Rock Eng.*, **52**(3), 691-718. https://doi.org/10.1007/s00603-018-1600-4.

Zhou, X.P., Bi, J. and Qian, Q.H. (2015), "Numerical simulation of crack growth and coalescence in rock-like materials containing multiple pre-existing flaws", *Rock Mech. Rock Eng.*, **48**(3), 1097-1114. https://doi.org/10.1007/ s00603-014-0627-4.

Zhu, Z., Li, Y., Xie, J. and Liu, B. (2015), "The effect of principal stress orientation on tunnel stability", *Tunn. Undergr. Sp. Technol.*, **49**, 279-286. https://doi.org/10.1016/j.tust.2015.05.009.

GC